Pergamon

Int. Comm. Heat Mass Transfer, Vol. 30, No. 3, pp. 423-433, 2003

0735–1933/03/$–see front matter

Available online at www.sciencedirect.com

SCIENCE DIRECT®

PII: S0735-1933(03)00060-5

THE EFFECT OF SUCTION BOUNDARY CONDITION ON THE LOCAL AND AVERAGE NUSSELT NUMBERS FOR A FREE CONVECTION FLOW REGIME

E. Abu-Nada, A. Al-Sarkhi, M. Ashhab, B. Akash
Department of Mechanical Engineering, Hashemite University
Zarqa 13115, Jordan
E-mail: eiyad@hu.edu.jo

(Communicated by J.P. Hartnett and W.J. Minkowycz)

ABSTRACT

This paper studies the effect of suction on local and average Nusselt number around a cylinder surface subjected to natural convection. The complete Navier-Stokes and energy equations are formulated in terms of stream function and vorticity. They are solved using the finite difference technique. The Rayleigh number is ranged between 1×10^3 to 1×10^5 in the current simulations. An increase in the overall Nusselt number with an increase in the suction flow rate for the three simulated Rayleigh numbers is reported. For the lowest simulated flow rate, i.e. Q = 5, the average Nusslet number difference between the three Ralyeigh number modeled cases is relatively significant. However for the maximum simulated suction flow rate, i.e. Q =40, the difference is relatively small. It is found that the location of the sharp drop of the Nusslet number is moved to a higher value of θ by increasing the suction flow rate. Also, the plume region size diminishes by increasing the value of Q. This behavior extends to a point, Q = 40, where the plume area disappears completely for the cases Ra = 1×10^3 and Ra = 1×10^4. Finally, the results designate a variation between the uniform and non uniform suction on the cylinder surface.

Introduction

The heat transfer from a horizontal heated cylinder has many engineering applications such as heat exchangers. Some types of heat exchangers depend on natural convection as the main heat transfer mechanism, while others depend on mixed or forced convection for heat removal. It is important to understand the thermal behavior of such systems when the forced external flow is absent and the only mechanism for heat transfer is by natural convection. The geometrical shape of the cylinder creates non-uniformity in the heat transfer around the cylinder surface. This variance leads to bad spots, where the cylinder ability to dissipate its heat to the surrounding fluid reduces; accordingly the heat transfer drops

significantly. With a better understanding of the flow field behavior around the cylinder, it is possible to devise methods for improving the heat transfer for these bad regions. One control technique that is used frequently, by researchers, is suction/blowing on the flow boundary layer. This procedure will be investigated in this article to enhance the heat transfer from the cylinder surface. The scope of this work is to impose suction around the cylinder surface to enhance the heat transfer from the cylinder surface and to reduce the non uniformity experienced in the classical natural convection case.

The natural convection from a horizontal circular cylinder has been investigated extensively. Previous researchers, such as Kuhen and Goldstien [1] solved the complete Navier-Stokes and energy equations for laminar natural convection about a horizontal isothermal cylinder using finite difference technique. Also, Farouk and Gucceri [2] solved the flow around the cylinder for uniform and non uniform temperature and heat flux distribution. Additionally, Qureshi and Ahmad [3] solved the flow for uniform heat flux and they compared their results with their own experiments. Moreover, Wang et al. [4] investigated the laminar natural convection flow using the spline fractional step method. The previous mentioned published work treated the cylinder surface as an impermeable surface, where no fluid can be sucked or blowed from the cylinder surface. In view of that, the previous mentioned published work did not focus on the effect of suction or blowing flow boundary condition on the amount of heat transfer from the cylinder surface. The current authors are not aware of any published work that addresses the effect of imposing suction, on the cylinder surface, on the local Nusselt number variation around the cylinder surface. The goal of this work is to study the effect of suction on the local and average Nusselt number along the cylinder surface. To accomplish this goal, the problem will be investigated numerically, where the complete Navier-Stokes and energy equations (NSE) are solved using the finite difference technique to describe the natural convection around the horizontal cylinder, subjected to suction on the cylinder surface. The NSE will be written in terms of stream function and vorticity formulation. Formulae for stream function and vorticity on the cylinder surface due to suction will be derived. In addition, the distribution of local and circumferential Nusselt around the cylinder will be analyzed.

Governing Equations and Problem Formulation

Fig. 1 shows a schematic diagram of the cylinder and the physical flow field. Due to the flow symmetry experienced for the natural convection case, half of the cylinder will be modeled, as shown in Fig. 2, which will reduce the computational time by half. The governing equations for the laminar steady state natural convection in terms of the stream function-vorticity formulation in a non-dimensional form [2, 5]:

$$\frac{\partial}{\partial r}\left(r\frac{\partial \psi}{\partial r}\right)+\frac{\partial}{\partial \theta}\left(\frac{1}{r}\frac{\partial \psi}{\partial \theta}\right)=-r\omega, \tag{1}$$

$$\frac{\partial}{\partial r}(\omega\frac{\partial\psi}{\partial\theta})-\frac{\partial}{\partial\theta}(\omega\frac{\partial\psi}{\partial r})=\Pr[\frac{\partial}{\partial r}(r\frac{\partial\omega}{\partial r})+\frac{\partial}{\partial\theta}(\frac{1}{r}\frac{\partial\omega}{\partial\theta})]+Ra\Pr[\frac{\partial T}{\partial r}\sin\theta+\frac{\partial T}{\partial\theta}\cos\theta]=0, \quad (2)$$

and

$$\frac{\partial}{\partial r}(T\frac{\partial\psi}{\partial\theta})-\frac{\partial}{\partial\theta}(T\frac{\partial\psi}{\partial r})=[\frac{\partial}{\partial r}(r\frac{\partial T}{\partial r})+\frac{\partial}{\partial\theta}(\frac{1}{r}\frac{\partial T}{\partial\theta})]. \quad (3)$$

The non dimensional parameters, introduced in the previous equations, are as defined in [7, 8]:

$$\psi=\frac{\overset{*}{\psi}}{\alpha},\ \omega=\frac{\overset{*}{\omega}R^2}{\alpha},\ T=\frac{\overset{*}{T}-T_\infty}{T_w-T_\infty}.$$

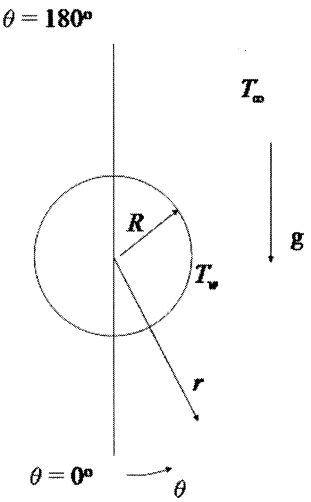

FIG. 1
Schematic diagram of the cylinder and the physical parameters.

The radial and tangential velocities are given by the following relations respectively,

$$u=\frac{1}{r}\frac{\partial\psi}{\partial\theta}, \text{ and} \quad (4)$$

$$v=-\frac{\partial\psi}{\partial r}. \quad (5)$$

A fine grid is needed in the regions that are close to the cylinder surface to resolve the boundary layer while a courser grid could be used far away from the cylinder surface This grid stretching method results in considerable savings in terms of the grid size and the computational time [6]. The stretched grid in the physical domain is further transformed into a uniformm grid in the computational domain using the following transformation of the dependent variables: $r=e^{\pi\xi}$, and $\theta=\pi\eta$. Fig. 2 shows the grid in both

the physical and computational domains, respectively. In the computational domain Eqs. (1)-(3) are rwritten as [7, 8]:

$$\frac{\partial^2\psi}{\partial\xi^2}+\frac{\partial^2\psi}{\partial\eta^2}=-E^2\omega, \tag{6}$$

$$\frac{\partial}{\partial\xi}(\omega\frac{\partial\psi}{\partial\eta})-\frac{\partial}{\partial\eta}(\omega\frac{\partial\psi}{\partial\xi})=\Pr[\frac{\partial^2\omega}{\partial\xi^2}+\frac{\partial^2\omega}{\partial\eta^2}]+Ra\Pr[\frac{\partial T}{\partial\xi}\sin\eta+\frac{\partial T}{\partial\eta}\cos\eta], \tag{7}$$

$$\frac{\partial}{\partial\xi}(T\frac{\partial\psi}{\partial\eta})-\frac{\partial}{\partial\eta}(T\frac{\partial\psi}{\partial\xi})=[\frac{\partial^2\omega}{\partial\xi^2}+\frac{\partial^2\omega}{\partial\eta^2}], \tag{8}$$

where: $E=\pi e^{\pi\xi}$.

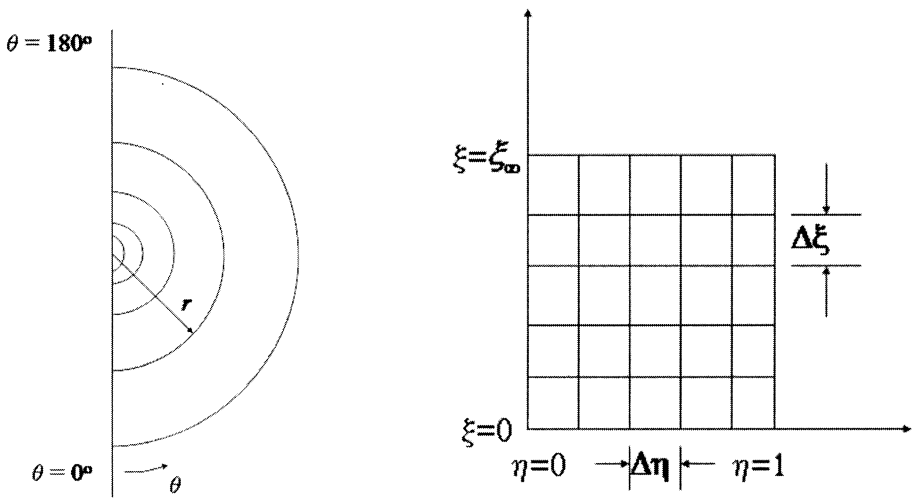

FIG. 2
Schematic diagram of the (a) physical and (b) computational domain.

Implementation of Boundary Conditions

An accurate representation of the stream function vorticity at the cylinder surface is the most critical step in the stream function vorticity formulation [9]. Thus, one has to be careful in selecting the correct formulae. In the present paper the suction velocity at the cylinder surface is used to derive correlations for the stream function at the cylinder surface. On the other hand, to derive formulae for the voriticity, Eq. (1) will be used in addition to the derived stream function formula. The derivation of the stream function starts by expressing the suction velocity at the cylinder surface in terms of the stream

function. The suction surface velocity, both in tangential and radial directions respectively, can be expressed in the computational domain by the following formulae:

$$\frac{\partial \psi}{\partial \eta} = u_s \pi \,, \tag{9}$$

$$\frac{\partial \psi}{\partial \xi} = 0 \,, \tag{10}$$

where u_s denotes the non-dimensional suction velocity at the cylinder surface. The boundary conditions for the stream function-vorticity formulation are written as:

1. At cylinder surface: ψ=0, $\omega = -\frac{1}{\pi^2}\left(\frac{\partial^2 \psi}{\partial \xi^2} + \frac{\partial^2 \psi}{\partial \eta^2}\right)$, and T = 1,

2. On symmetry line, i.e. η = 0 and η = 1: ψ=0, ω=0, and $\frac{\partial T}{\partial \eta} = 0$.

3. Faraway boundary: $\frac{\partial^2 \psi}{\partial \xi^2} = 0$, T= 0, and $\omega = -\frac{1}{E^2}\frac{\partial^2 \psi}{\partial \eta^2}$.

All the governing equations, Eq. (6) – Eq. (8) are discritized using second order central finite difference formulas for the interior points. Accordingly, to get the same kind of accuracy on the boundaries, the boundary conditions on the cylinder surface and faraway boundary are also discritized using second order forward or backward difference formulas, respectively. The second order accurate stream function at the cylinder surface is implemented by using the expression given by Eq. (9). By applying this, we get

$$\psi_{j+1} = \psi_{j-1} + 2\pi \Delta \eta u_s \,, \tag{11}$$

where j+1 and j-1 are two grid points surrounding the control volume centered at the grid point j, where the suction velocity u_s is imposed. Numerical implementation of Eq. (11) starts from the lower symmetry line of the cylinder, i.e. η = 0, by setting the value of ψ to zero. Then, we use the value of suction velocity at the cylinder surface, to calculate the stream function at each grid point on the cylinder surface. Accordingly, the total suction flow rate on the cylinder surface can be calculated by summing all the suction flow rates on the control volumes. The suction on each control volume is expressed as $Q_{cv} = u_s \Delta \eta$, where $\Delta\eta$ is the tangential spacing in the computational domain. See Fig. 2. Thus, the total suction flow rate on the cylinder is equal to the suction velocity of the control volume, i.e. $Q'_{cv} = u_s$. The amount of suction flow rate that is used in the current analysis is defined by the following formula $Q = \pi Q'_{cv}$. Also, using the non-dimensional definition of velocity for the suction velocity u_s, we can express u_s in terms of the non-dimensional Reynolds and Prandtl number as $u_s = \mathrm{Re}\,\mathrm{Pr}$. Therefore, the amount of suction flow rate imposed, in the current simulations, at the cylinder surface is equal

to $Q = \pi \operatorname{Re}\operatorname{Pr}$. After we obtained the stream function at the cylinder surface we should be able to derive the appropriate vorticity boundary condition. The finite difference representation of the vorticity can be done by expressing the two terms $\frac{\partial^2\psi}{\partial\xi^2}$ and $\frac{\partial^2\psi}{\partial\eta^2}$, in Eq. (6), in second order accurate formulae.

The term $\frac{\partial^2\psi}{\partial\xi^2}$ can be expressed by the follwoing formula [8]

$$\omega_\xi = \frac{2\left(\psi_{1,j} - \psi_{0,j}\right)}{\left(\Delta\xi\right)^2}. \tag{12}$$

Using Eq. (11), the second term can be expressed as

$$\frac{\partial^2\psi}{\partial\eta^2} = \frac{2\pi\Delta\eta u_s + 2\psi_{j-1} - 2\psi_j}{\left(\Delta\eta\right)^2}. \tag{13}$$

The stream function at the cylinder surface can be expressed, by using Eq. (10) and second order accurate forward difference formulae for the first velocity derivative, as [6]:

$$\psi_{0,j} = \frac{4}{3}\psi_{1,j} - \frac{1}{3}\psi_{2,j}$$

Thus, Eq. (13) is rewritten as:

$$\frac{\partial^2\psi}{\partial\eta^2} = \frac{2\pi\Delta\eta u_s + 2\psi_{j-1} - \frac{2}{3}\left(4\psi_{1,j} - \psi_{2,j}\right)}{\left(\Delta\eta\right)^2}. \tag{14}$$

Substituting Eq. (12) and Eq. (14) into Eq. (6), the final form of the vorticity at the cylinder surface can be expressed as

$$\omega_\xi = -\frac{1}{\pi^2}\left(\frac{2\left(\psi_{1,j} - \psi_{0,j}\right)}{\left(\Delta\xi\right)^2} - \frac{2}{3(\Delta\eta)^2}\left(4\psi_{1,j} - \psi_{2,j}\right) + \frac{2\left(\pi\Delta\eta u_s + \psi_{0,j-1}\right)}{\left(\Delta\eta\right)^2}\right) \tag{15}$$

Numerical Model

The finite difference equations in the present work were solved using an explicit iterative method and the residual concept. The equations for T, ψ, and ω are written, by using the residual concept, in the following form:

$$resid = \frac{RF(a_{i,j}Y^{m-1}_{i,j+1} + bb_{i,j}Y^{m-1}_{i,j-1} + c_{i,j}Y^{m-1}_{i+1,j} + d_{i,j}Y^{m-1}_{i-1,j} + ST)}{e_{i,j}} - RF(Y^{m-1}_{i,j}), \tag{16}$$

where $Y_{i,j}$ denotes either ψ, ω, or ϕ. The subscript (m-1) denotes estimates calculated from the previous iteration. An under relaxation factor was used when calculating the new estimates for ψ, ω, and ϕ. This is

done in order to avoid the problem of divergence due to the non-linear terms in the equations. The iterations were continued until the overall error was less than ε. The value of ε in the present study was set to 1×10^{-6}, which gave no significance change in the final solution with any value less than this number [7]. The convergence criteria were defined by the following expression:

$$\varepsilon = \frac{\sum_{j=1}^{j=M}\sum_{i=1}^{i=N}\left|\text{resid}_{i,j}\right|}{\left|\sum_{j=1}^{j=M}\sum_{i=1}^{i=N}L_{i,j}\right|} \tag{17}$$

where $L_{i,j}$ denotes either ψ, ω, or ϕ , and M and N are the number of grid points both in tangential and radial directions respectively. The code for this current work was validated, in previous work, for the case with no suction, against experimental and theoretical published data [8]. The validation was against Nusselt number variation along the cylinder surface and flow the tangential velocity. Our code showed excellent validation against the mentioned published data. The disctritized form of the local Nusselt number is written as:

$$Nu_D = -\frac{1}{\pi\Delta\xi}(-3T_{1,j} + 4T_{2,j} - T_{3,j}). \tag{18}$$

The average Nusselt number is defined as:

$$\overline{\text{Nu}}_D = \frac{1}{\pi}\int_0^{\pi}\text{Nu}_\theta d\theta \tag{19}$$

A 1/3[rd] Simpson's rule of integration is used to evaluate Eq. (18).

Results and Discussion

The Rayleigh number is ranged between 1×10^3 to 1×10^5 in the current simulations. Fig. 3 shows the variation of the average Nusselt number with the suction flow rate. The figure records an increase in the overall Nusselt number with an increase in the suction flow rate for the three simulated Rayleigh number curves. For the lowest simulated flow rate, i.e. Q = 5, the average Nusslet number difference between the three curves is higher than that of the maximum simulated suction flow rate, i.e. Q =40. This behavior can be explained by looking at the physics of the problem. The physics indicates that a combined action of natural and forced suction convection are presented, where at lower values of Q both the natural convection and forced suction are of the same order of influence. However, for larger values of Q, i.e. Q=40, the action of forced suction dominates over the natural convection. Thus, the values of Nusselt number at higher values of Q are mostly contributed from the forced suction, which is the reason for the less dependence of Nusselt number on the Rayleigh number.

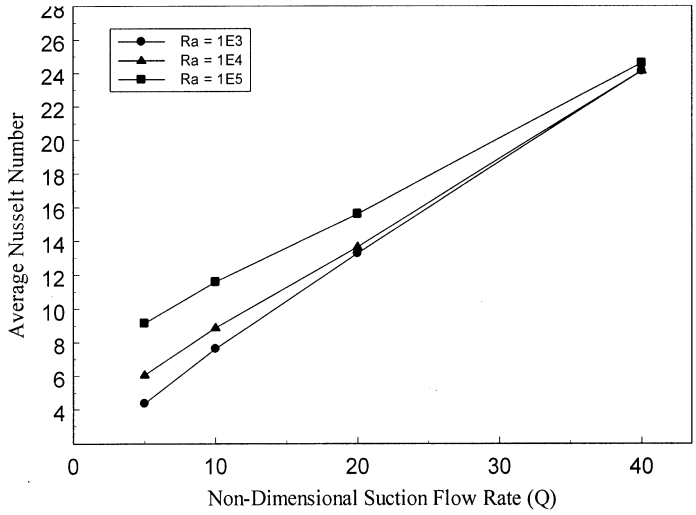

FIG. 3
Average Nusselt number variation with the suction flow rate for three different Rayleigh Numbers.

Fig. 4 shows the circumferential change of the local Nusslet number on the surface. The figure shows an additional interesting behavior, where place of the sharp drop of the Nusslet number is moved to a higher value of θ. That means the bad regions of heat transfer are narrowed down by increasing the value of Q.

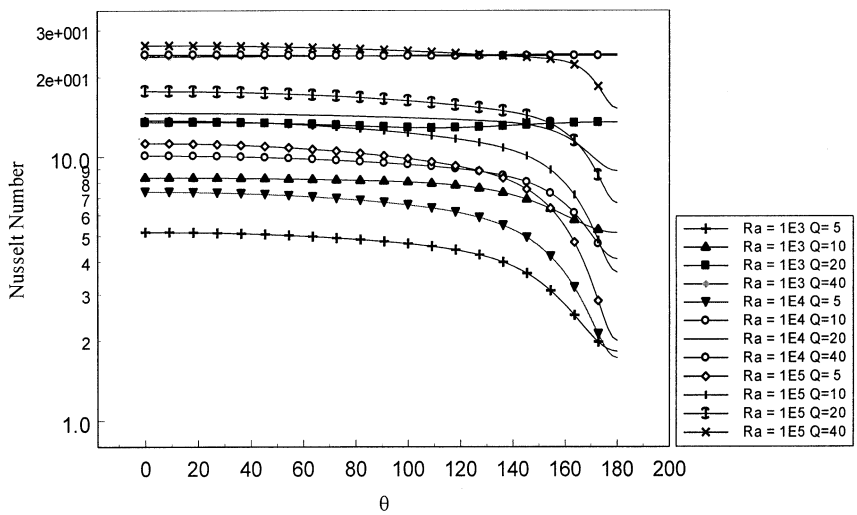

FIG. 4
Circumferential variation of Nusselt number.

This behavior is also emphasized by Fig. 5, where the plume, the bad heat transfer areas, starts to diminish by increasing the value of Q. This behavior extends to a point, Q = 40, where the plume area is completely disappear. The disappearance of the plume region is also clearly predicted in Fig. 4 by the flat curve behavior for Q =40 and Ra=1E3, 1E4.

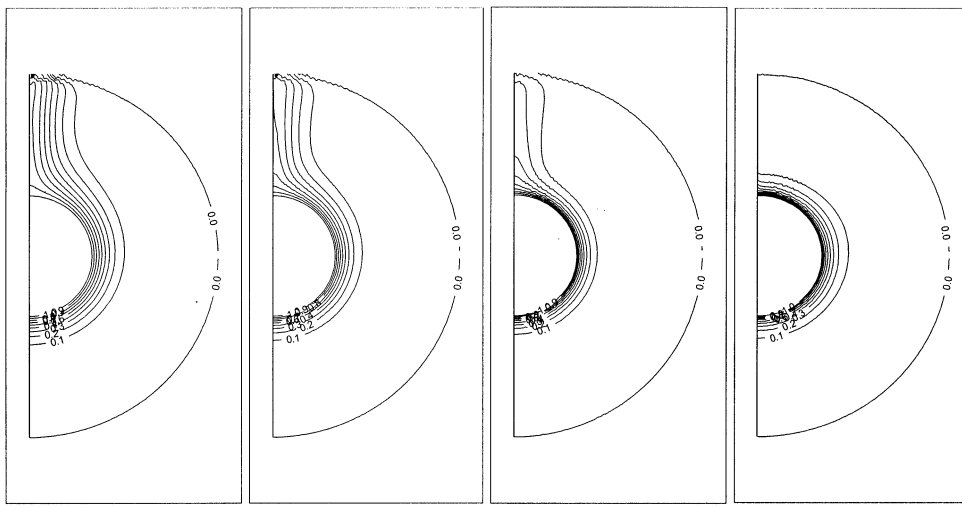

(a) (b) (c) (d)

FIG. 5
Temperature contour plots for Ra = 1E4 (a) Q = 5 (b) Q = 10, (c) Q = 20 (d) Q = 40

Fig. 6 shows another scenario for the variation of the average Nusselt number with the suction flow rate, but for a non uniform suction case. In this case, the cylinder is divided into two parts, where the suction flow rate is doubled in the upper half of the cylinder compared to the lower half. The figure designates a variation between both cases, i.e. for the uniform and non uniform suction.

Conclusions

The change of Nusslet number, average and local, around a horizontal isothermal cylinder subjected to natural convection with suction is studied numerically. There is a direct proportional increase in the average Nusselt number values with increasing the suction flow rate. The plume region area decreases as the suction flow rate increases and eventually disappears at high values of Q. When the suction flow rate is doubled in the upper half of the cylinder over the lower half of the cylinder a direct increase in the Nusslet number is reported. This work could be extended for future work to incorporate a turbulence regime to predict the effect of suction on the Nusselt number for a turbulent case.

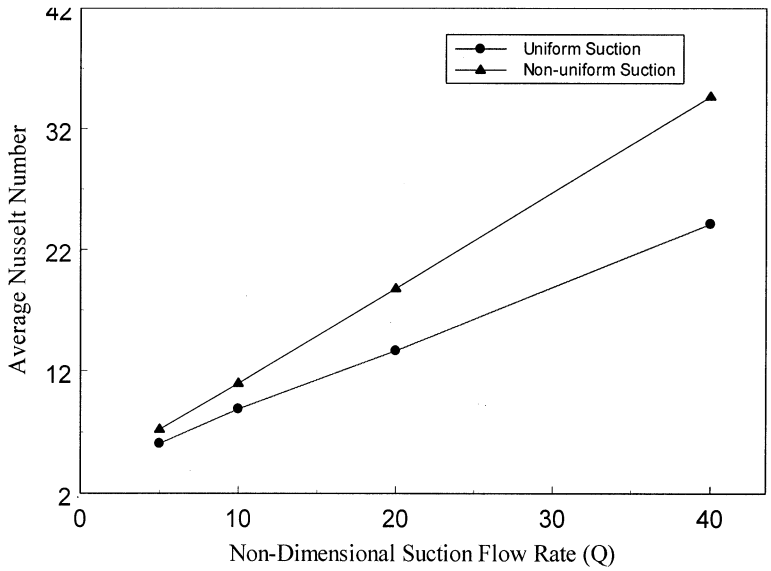

FIG. 6
Average Nusselt number variation with the no uniform suction flow rate for Ra = 10000

Nomenclature

h	Local heat transfer coefficient
k	Thermal conductivity
Nu_D	Nusselt number based on diameter, Nu = hD/k
Pr	Prandtl number
Q	Modified total suction flow rate on the cylinder surface, used in the current simulation.
Q'	Total suction flow rate on the cylinder surface.
R	Radius of the cylinder
r^*	Radial coordinate measured from the cylinder of the cylinder
r	Non dimensional radial distance, r/R.
Ra	Rayleigh number based on diameter, $g\beta D^3(T_s - T_\infty)/(\nu\alpha)$
Re	Reynolds number based on radius, Re=$\alpha u_s/\nu$
T^*, T	Dimensional and non-dimensional temperatures respectively
u^*	Dimensional radial velocity
u	Non-dimensional radial velocity, $u = u^* D/\alpha$
u_s^*	Dimensional suction velocity on the cylinder surface
u_s	Non dimensional suction velocity on the cylinder surface, $u_s = u_s^* D/\alpha$
v^*	Tangential velocity

v	Non dimensional tangential velocity, $v = \overset{*}{v}D/\alpha$
α	Thermal diffusivity
β	Coefficient of thermal expansion
η, ξ	Coordinates in computational plane
θ	Angle measured from the lower symmetry plane
ψ	Stream function
ω	vorticity

References

1. T. H. Kuhen, and R. J. Goldstein, *Int. J. Heat Mass Transfer* **23**, 971-979 (1980).
2. B. Farouk, and S. I. Guuceri, *J. Heat Transfer* **103**, 522-527 (1981).
3. Z. H. Qureshi, and R. Ahmad, *Num. Heat Transfer* **11**, 199-212 (1987).
4. P. Wang, R. Kahawita, and T. H. Nguyen, *Num. Heat Transfer* **17**, part A, 191-215 (1990).
5. F. M. White, *Viscous Fluid Flow*, 2nd ed., McGraw-Hill, New York (1974).
6. J. D. Anderson, *Computational Fluid Dynamic: The Basics with Applications*, McGraw-Hill, New York, (1995).
7. B. A/K Abu-Hijleh, M. Abu-Qudais, and E. Abu Nada, *J. Heat Transfer* **120**, 1089-1091 (1998).
8. B. A/K Abu-Hijleh, M. Abu-Qudais, and E. Abu Nada, *Energy*, **24**, 327-333 (1999).
9. V. S. Arpaci, and P. S. Larsen, *Convection Heat Transfer*, Prentice-Hall, Englewood Cliffs (1984).

Received December 2, 2002